# Photophysical and Photocatalytic Properties of $MIn_{0.5}Nb_{0.5}O_3$ (M = Ca, Sr, and Ba)

**Jiang Yin,*,† Zhigang Zou,‡ and Jinhua Ye†**

*Ecomaterials Center, National Institute for Materials Science (NIMS), 1-2-1 Sengen, Tsukuba, Ibaraki 305-0047, Japan, and Photoreaction Control Research Center (PCRC), National Institute of Advanced Industrial Science and Technology (AIST), 1-1-1 Higashi, Tsukuba, Ibaraki 305-8565, Japan*

*Received: June 28, 2002; In Final Form: October 8, 2002*

New photocatalysts $MIn_{0.5}Nb_{0.5}O_3$ (M = Ca, Sr, and Ba) with the $ABO_3$ type perovskite structure in which B sites are occupied by $In^{3+}$ or $Nb^{5+}$ ions randomly in a charge-balanced manner were synthesized. They were characterized by structural analysis, diffuse reflectance spectroscopy, and photocatalytic activity measurement in evolving $H_2$ and $O_2$ from pure water with cocatalysts Pt and $NiO_x$ under UV and visible light irradiation ($\lambda > 420$ nm), respectively. It is suggested that the conduction bands of these photocatalysts are composed of In 5s and Nb 4d levels, and the valence bands are composed of O 2p levels. With the decrease of the ionic radius in the A site, the $CaIn_{0.5}Nb_{0.5}O_3$, $SrIn_{0.5}Nb_{0.5}O_3$, and $BaIn_{0.5}Nb_{0.5}O_3$ photocatalysts show different photocatalytic activities. Under UV light irradiation, the $BaIn_{0.5}Nb_{0.5}O_3$ photocatalyst powder with cocatalyst $NiO_x$ split pure water into $H_2$ and $O_2$ in a nearly stoichiometric ratio. Under visible irradiation, all of these photocatalysts show obvious photocatalytic activity in evolving $H_2$ from pure water with cocatalyst $NiO_x$.

## 1. Introduction

Since photoinduced decomposition of water on a $TiO_2$ electrode was discovered by Honda et al.,[1] semiconductor-based photocatalysis has attracted much interest due to the prospect of conversion of solar energy to chemical energy stored in gaseous hydrogen. Several types of semiconductor photocatalysts such as simple oxides ($Nb_2O_5$, $Ta_2O_5$, and $ZrO_2$, etc.) as well as some simple perovskite or modified perovskite oxides ($SrTiO_3$, $SrNb_2O_7$, and $SrTa_2O_7$, etc.) have been developed for $H_2$ and $O_2$ production from water or other aqueous solutions.[2−4] It was thought that niobium- or tantalum-based oxides with perovskite type structures would show high photocatalytic activities in splitting water into $H_2$ and $O_2$ under UV light irradiation, due to the fact that the formed $NbO_6$ or $TaO_6$ octahedral chains or layers favor a possible delocalization of charge carriers. To effectively use the energy of sunlight, it is desirable to develop new photocatalysts with a $NbO_6$ (or $TaO_6$) octahedral structure and narrower band gap (less than 3.0 eV) in order to split water into $H_2$ and $O_2$ under visible light irradiation. The first route may be donor-doping or acceptor-doping in the semiconductor photocatalysts to produce an intermediate energy level, thus reducing the actual band gap. Generally, niobium-based oxides such as $Sr_2Nb_2O_7$ have such wide band gaps (>4.0 eV) that the first route is almost ineffective. Thus, inserting an intermediate energy level inside the wide band gap of the semiconductor directly may be a possible route. Here, the synthesis and the photocatalytic activities of the new photocatalysts $MIn_{0.5}Nb_{0.5}O_3$ (M = Ca, Sr, and Ba) with simple $ABO_3$ type perovskite structures in which B sites are occupied by two kinds of metal ions randomly in a charge-balanced manner (CBM) are reported.

## 2. Experimental Section

Polycrystalline powders of $CaIn_{0.5}Nb_{0.5}O_3$, $SrIn_{0.5}Nb_{0.5}O_3$, and $BaIn_{0.5}Nb_{0.5}O_3$ were synthesized by a solid state reaction method. The predried $CaCO_3$, $SrCO_3$, $BaCO_3$, $In_2O_3$, and $Nb_2O_5$ powders with high purity in chemical stoichiometry were mixed thoroughly and calcined at 850 °C for 8 h. The preheated mixtures were reground and then sintered at 1230 °C for 48 h. The crystal structures of these ceramic powders were determined by X-ray powder diffraction (JEOL JDX-3500, Tokyo, Japan). UV−vis reflectance spectra of the photocatalysts were measured by an UV−vis spectrometer (Shimadzu UV-2500PC, Tokyo, Japan). The photocatalytic reactions were examined using a closed gas circulation system. A 300 W Xe arc lamp was focused through a shutter window, and a 420 nm cutoff filter was placed onto the window face of the cell. The photocatalytic activity for these photocatalyst powders under UV light irradiation was examined using an inner irradiation type quartz cell with a 400 W high-pressure Hg lamp. The gas evolved was determined with a TCD gas chromatograph (Shimadzu GC-8A, Tokyo, Japan), which was connected to the system with a circulating line. Just like the photocatalytic reaction for $TiO_2$, Pt was loaded on the surface of the photocatalyst in order to obtain high activity.[5,6] In addition, 1.0 wt % $NiO_x$ was also loaded on the surface of the photocatalyst powder from aqueous $Ni(NO_3)_2$ solution. The Ni-loaded photocatalysts were calcined at 500 °C for 1 h and then calcined at 500 °C for 2 h in a mixed atmosphere of Ar and $H_2$ (Ar:$H_2$ = 9:1 in volume). Finally, the $H_2$-treated photocatalysts were calcined at 200 °C for 1 h in pure $O_2$ atmosphere in order to get the $NiO_x$/Ni bilayer structure on the surface of the photocatalysts.[7] $H_2$ evolution reactions were performed in aqueous $CH_3OH/H_2O$ solution with cocatalyst Pt (0.5 g of 0.2 wt % Pt-loaded powder photocatalyst, 50 mL of $CH_3OH$, 220 mL of $H_2O$ under visible light irradiation or 320 mL of $H_2O$ under UV light irradiation). $O_2$ evolution reactions were performed in aqueous $AgNO_3$ solution without any cocatalyst (0.5 g photocatalyst, 5 mmol $AgNO_3$, 270 mL

† National Institute for Materials Science (NIMS).
‡ National Institute of Advanced Industrial Science and Technology (AIST).

10.1021/jp026403y CCC: $25.00 
Published on Web 12/03/2002

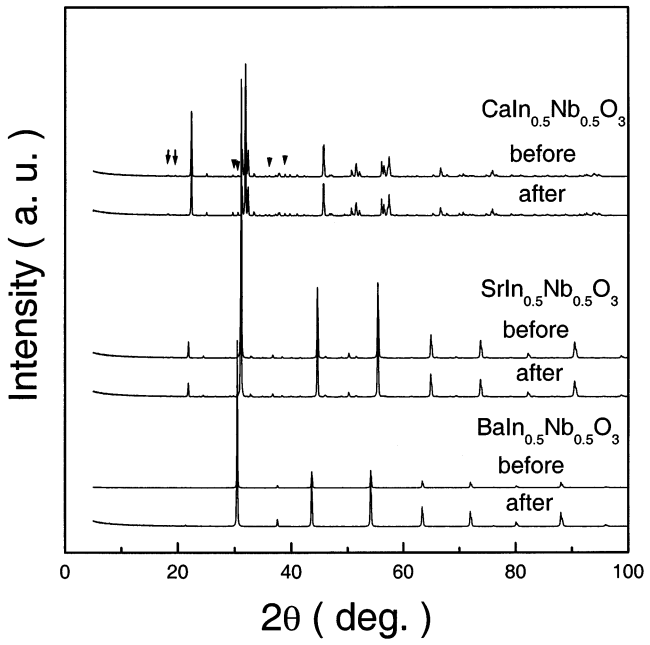


**Figure 1.** X-ray powder diffraction patterns for the $CaIn_{0.5}Nb_{0.5}O_3$, $SrIn_{0.5}Nb_{0.5}O_3$, and $BaIn_{0.5}Nb_{0.5}O_3$ photocatalysts before and after $H_2$ evolution reactions from $CH_3OH/H_2O$ solutions under UV light irradiation, where impurity phases were indicated by the arrows.

of $H_2O$ under visible light irradiation or 370 mL of $H_2O$ under UV light irradiation). The surface areas of the powder samples were measured by the Brunauer−Emmett−Teller (BET) method.

## 3. Results and Discussion

**3.1. Structural Analysis.** X-ray powder diffraction patterns for the photocatalysts $CaIn_{0.5}Nb_{0.5}O_3$, $SrIn_{0.5}Nb_{0.5}O_3$, and $BaIn_{0.5}Nb_{0.5}O_3$ are shown in Figure 1. $SrIn_{0.5}Nb_{0.5}O_3$ and $BaIn_{0.5}Nb_{0.5}O_3$ powders were well-crystallized with simple perovskite phases, and some unknown phases were observed for $CaIn_{0.5}Nb_{0.5}O_3$ powders, as indicated by the arrows in Figure 1. The intensity of the strongest diffraction peak for the impurity phase is only 2.5% of that for the $CaIn_{0.5}Nb_{0.5}O_3$ phase. It means that the impurity phase will not significantly modify the properties of the $CaIn_{0.5}Nb_{0.5}O_3$ photocatalyst. For an ideal $A^{2+}B^{4+}O_3$ type perovskite structure such as $CaTiO_3$, the corners of the cubic cell are occupied by $A^{2+}$ ions with coordination number 12 and the sites of the face centers are occupied by $O^{2-}$ ions with coordination number 6. The bulk center is occupied by the $B^{4+}$ ion with coordination number 6. $B^{4+}$ and six neighboring $O^{2-}$ ions form an octahedron $BO_6$. The neighboring octahedrons are connected to each other by sharing the corner to form a three-dimensional octahedron network. Here, for $CaIn_{0.5}Nb_{0.5}O_3$, $SrIn_{0.5}Nb_{0.5}O_3$, and $BaIn_{0.5}Nb_{0.5}O_3$ perovskite structures, the sites of the bulk center are occupied randomly by $In^{3+}$ and $Nb^{5+}$ ions in a CBM, which has been widely investigated for ferroelectric materials.[8,9] There is the following relationship among the radii of three ions $A^{2+}$, $B^{4+}$, and $O^{2-}$:

$$r_A + r_O = t\sqrt{2}(r_B + r_O) \quad (1)$$

where $t$ is defined as the tolerance factor.[10] The tolerance factor $t$ for a stable cubic perovskite structure is about 0.77−1.10. If the cation radius or the temperature changes, the symmetry of the perovskite structure may decrease. From $Ba^{2+} \rightarrow Sr^{2+} \rightarrow Ca^{2+}$, the ionic radius changes from 1.61 → 1.44 → 1.34 Å, respectively, and correspondingly, the crystal structure changes from a cubic → cubic → orthorhombic structure for $MIn_{0.5}Nb_{0.5}O_3$ (M = Ba, Sr, and Ca), while the tolerance factor changes from 0.99 → 0.93 → 0.90, respectively. It means that $ABO_3$ type compounds of stable cubic structure with CBM occupation in B sites probably possess a shorter region of tolerance factor.

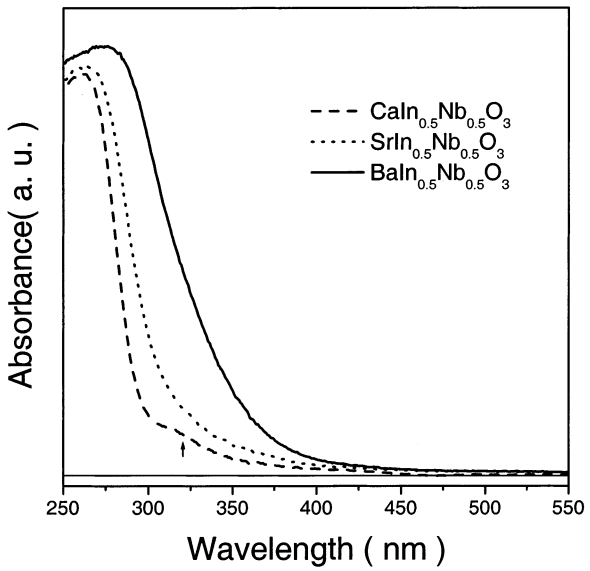


**Figure 2.** UV−vis diffuse reflectance spectra of the $CaIn_{0.5}Nb_{0.5}O_3$, $SrIn_{0.5}Nb_{0.5}O_3$, and $BaIn_{0.5}Nb_{0.5}O_3$ photocatalyst powders.

**3.2. UV−Vis Diffuse Reflectance Spectra.** Figure 2 shows the UV−vis diffuse reflectance spectra of $CaIn_{0.5}Nb_{0.5}O_3$, $SrIn_{0.5}Nb_{0.5}O_3$, and $BaIn_{0.5}Nb_{0.5}O_3$ ceramic powders. The values of the band gaps for these materials were evaluated by extrapolations of the straight regions of the absorption coefficient $\alpha^2$ vs photo energy $h\nu$, as adopted by Kim et al.[12] The band gaps for $CaIn_{0.5}Nb_{0.5}O_3$, $SrIn_{0.5}Nb_{0.5}O_3$, and $BaIn_{0.5}Nb_{0.5}O_3$ as determined are 4.17, 3.96, and 3.51 eV, respectively. Because of the decrease of the cation radius in the A site, $SrIn_{0.5}Nb_{0.5}O_3$, with a shorter lattice parameter, shows a wider band gap than $BaIn_{0.5}Nb_{0.5}O_3$, because of the relationship between the band gap and the lattice parameter a for cubic structure $E_g \propto 1/a^2$. $CaIn_{0.5}Nb_{0.5}O_3$, with a distorted perovskite structure and the smallest ionic radius in the A site, possesses the widest band gap. It is also obvious from Figure 2 that all of the spectra show long tails into the visible light region, which are ascribed to their special band structures. The band structure of a transition metal oxide with perovskite structure is generally defined by the d level of the transition metal and the O 2p level.[13] However, for the metal oxides containing a metal ion with $d^{10}$ electronic configuration, the conduction bands are not formed by their d levels. Theoretical calculations showed that the band features of the indium oxides with $InO_6$ octahedrons are dominated by the O 2p level and the In 5s level.[14,15] So, it is suggested that the band structures of $CaIn_{0.5}Nb_{0.5}O_3$, $SrIn_{0.5}Nb_{0.5}O_3$, and $BaIn_{0.5}Nb_{0.5}O_3$ are composed of In 5s level and O 2p level. The empty Nb 4d level is only the second conduction band. The absorption spectra of $CaIn_{0.5}Nb_{0.5}O_3$, $SrIn_{0.5}Nb_{0.5}O_3$, and $BaIn_{0.5}Nb_{0.5}O_3$ ceramic powders in the UV light region are dominated by the electronic excitation from O 2p states to Nb 4d states, and the absorption spectra in the visible light region are dominated by the electronic excitations from O 2p states to In 5s states. The shoulder around 320 nm in the diffuse reflectance spectrum of $CaIn_{0.5}Nb_{0.5}O_3$, as indicated by the arrow in Figure 2, is from the overlap of the different optical absorptions.

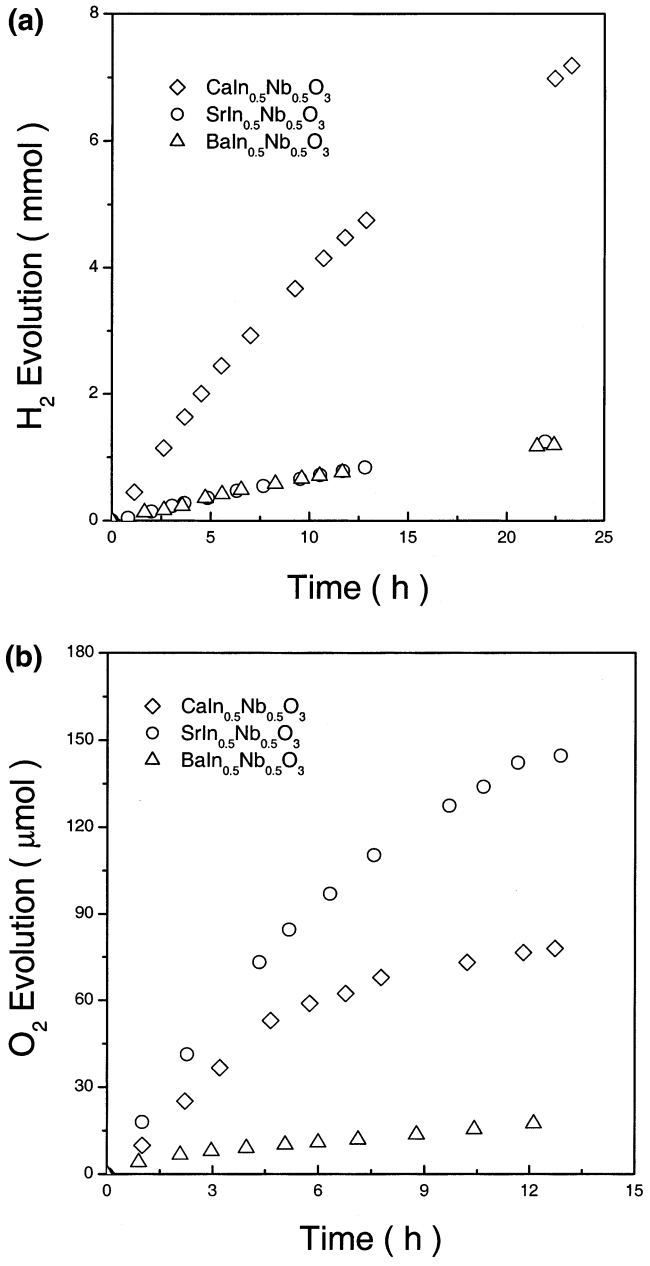


**Figure 3.** (a) Formation rates of $H_2$ evolution from $CH_3OH/H_2O$ solution with Pt cocatalyst (catalyst: 0.5 g; cocatalyst: 0.2 wt % Pt; $CH_3OH$, 50 mL; $H_2O$, 320 mL) and (b) formation rates of $O_2$ evolution from $AgNO_3$ solution (catalyst: 0.5 g; $AgNO_3$, 5 mmol; $H_2O$, 370 mL) for the $CaIn_{0.5}Nb_{0.5}O_3$, $SrIn_{0.5}Nb_{0.5}O_3$, and $BaIn_{0.5}Nb_{0.5}O_3$ photocatalysts under UV light irradiation.

**3.3. Photocatalytic Reactions under UV Light Irradiation.** The formation rates of $H_2$ evolution from $CH_3OH/H_2O$ solution with cocatalyst Pt (0.2 wt %) under UV light irradiation are shown in Figure 3a. For the $CaIn_{0.5}Nb_{0.5}O_3$ photocatalyst, the total amount of the $H_2$ evolved in the first 20 h is more than 7000 $\mu$mol, indicating a formation rate of 304 $\mu$mol/h. However, for the $SrIn_{0.5}Nb_{0.5}O_3$ and $BaIn_{0.5}Nb_{0.5}O_3$ photocatalysts, the total amounts of the $H_2$ evolved in the first 20 h are much less than that for the $CaIn_{0.5}Nb_{0.5}O_3$ photocatalyst, with formation rates of 57 and 51 $\mu$mol/h, respectively. The crystal structures of the $CaIn_{0.5}Nb_{0.5}O_3$, $SrIn_{0.5}Nb_{0.5}O_3$, and $BaIn_{0.5}Nb_{0.5}O_3$ photocatalysts after the $H_2$ evolution reactions were checked by the X-ray powder diffraction again, as shown in Figure 1. No additional phases were formed after $H_2$ evolution reactions for any sample. It means that $H_2$ evolution from $CH_3OH/H_2O$ solution with cocatalyst Pt under UV light irradiation is not from the chemical reaction between these ceramic powders and water. Figure 3b shows the formation rates of $O_2$ evolution from $AgNO_3$ solution (5 mmol $AgNO_3$) without any cocatalyst for $CaIn_{0.5}Nb_{0.5}O_3$, $SrIn_{0.5}Nb_{0.5}O_3$, and $BaIn_{0.5}Nb_{0.5}O_3$ photocatalysts under UV light irradiation. The formation rate of the $O_2$ evolution from $AgNO_3$ solution for $CaIn_{0.5}Nb_{0.5}O_3$ in the first 10 h is about 6.9 $\mu$mol/h, and those for $SrIn_{0.5}Nb_{0.5}O_3$ and $BaIn_{0.5}Nb_{0.5}O_3$ photocatalysts are about 12.0 and 1.2 $\mu$mol/h, respectively. Figure 3a,b indicates that the band structures of these photocatalysts meet the electrochemical requirements for photocatalytic water splitting reactions, i.e., the potential of the bottom of the conduction band is more negative than the redox potential of $H^+/H_2$ (0 V vs SHE, pH = 0), and the potential of the top of the valence band is more positive than the redox potential of $O_2/H_2O$ (1.23 V vs SHE, pH = 0). Just as suggested for other $ABO_3$ type perovskite compounds such as titanate,[16] with the decrease of the ionic radius in the A site, the potential of the conduction band for the compound will be elevated and the potential of the valence band will be lowered. A photocatalyst with a more negative potential at the bottom of the conduction band will show higher photocatalytic activity in evolving $H_2$ from water, and a photocatalyst with more positive potential at the top of the valence band will show higher photocatalytic activity in evolving $O_2$ from water. From Figure 3a, with the decrease of the ionic radius in the A site, the formation rates of $H_2$ evolution for the $CaIn_{0.5}Nb_{0.5}O_3$, $SrIn_{0.5}Nb_{0.5}O_3$, and $BaIn_{0.5}Nb_{0.5}O_3$ photocatalysts under UV light irradiation show a periodic trend. From Figure 3b, with the decrease of the ionic radius in the A site, the formation rate of $O_2$ evolution for $SrIn_{0.5}Nb_{0.5}O_3$ is larger than that for $BaIn_{0.5}Nb_{0.5}O_3$. The formation rate of $O_2$ evolution for $CaIn_{0.5}Nb_{0.5}O_3$ does not follow the periodic rule, even though the $CaIn_{0.5}Nb_{0.5}O_3$ photocatalyst powder possesses the largest surface area. The BET measurements show that the surface areas for the $CaIn_{0.5}Nb_{0.5}O_3$, $SrIn_{0.5}Nb_{0.5}O_3$, and $BaIn_{0.5}Nb_{0.5}O_3$ photocatalysts powders are 2.25, 1.93, and 1.71 $m^2/g$, respectively. This anomaly in the photocatalytic activity of $CaIn_{0.5}Nb_{0.5}O_3$ may be related to its different crystal structure and special surface state.

Figure 4 shows the formation rates of $H_2$ and $O_2$ evolution from the $NiO_x$-loaded $MIn_{0.5}Nb_{0.5}O_3$ (M = Ba, Sr, and Ca) particles suspended in pure water under UV light irradiation. The formation rates of $H_2$ evolution for the $CaIn_{0.5}Nb_{0.5}O_3$, $SrIn_{0.5}Nb_{0.5}O_3$, and $BaIn_{0.5}Nb_{0.5}O_3$ photocatalysts are 14.8, 13.8, and 27.0 $\mu$mol/h in the first 12 h, respectively. With the decrease of the ionic radius in the A site, the formation rates of $H_2$ evolution for these photocatalysts show no periodic trend, which may also be related to their different crystal and electronic structures, as well as special surface states of these photocatalyst particles. In our experiments, no $O_2$ evolution was observed for $CaIn_{0.5}Nb_{0.5}O_3$. In the first several hours, $O_2$ evolution was observed for $SrIn_{0.5}Nb_{0.5}O_3$, but as time passed, the total amount of $O_2$ evolved decreased, and finally, no $O_2$ could be detected by the instrument. For the $BaIn_{0.5}Nb_{0.5}O_3$ photocatalyst powder, $H_2$ and $O_2$ evolution in a ratio of 2.2:1 was observed at the same time, as shown by the inset in Figure 4.

Why oxygen evolution from pure water with the $NiO_x$-loaded $CaIn_{0.5}Nb_{0.5}O_3$ and $SrIn_{0.5}Nb_{0.5}O_3$ photocatalyst particles could not be steadily observed is not very clear. A series of works performed on other photocatalysts may provide some helpful clues. It was believed that free holes in $TiO_2$ particles can generate OH radicals, either on the surface or even at the aqueous interface.[17,18] Other researchers found that by low-energy photon irradiation there are both physisorbed and

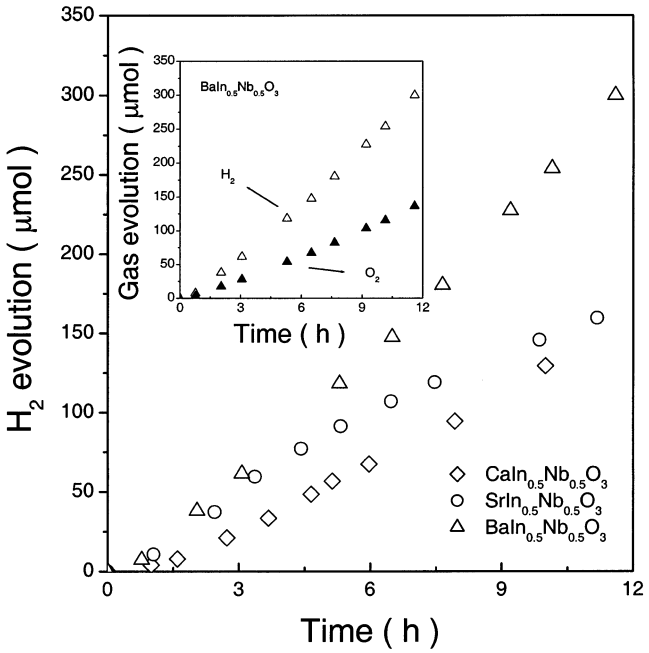


**Figure 4.** Formation rates of $H_2$ and $O_2$ evolution from $NiO_x$-loaded $CaIn_{0.5}Nb_{0.5}O_3$, $SrIn_{0.5}Nb_{0.5}O_3$, and $BaIn_{0.5}Nb_{0.5}O_3$ particles suspended in pure water under UV light irradiation (catalyst: 0.5 g; $NiO_x$, 1.0 wt %; $H_2O$, 370 mL).

chemisorbed oxygen molecules on the $TiO_2$ surface,[19,20] where the physisorbed $O_2$ molecules are produced through the neutralization of chemisorbed $O_2^-$ species by photogenerated holes. Zou et al.[21] measured the dc magnetic susceptibilities of the transition metal oxide $Bi_2InNbO_7$ with $InO_6$ and $NbO_6$ octahedrons before and after the photocatalytic reactions and found that the magnetic susceptibility of $Bi_2InNbO_7$ photocatalyst after the photocatalytic reactions showed an obvious broad peak around 50 K, which was ascribed to the antiferromagnetic ordering of adsorbed oxygen on the surface of the sample. For most oxide materials, the physisorbed and chemisorbed oxygen molecules will exchange with the oxygen vacancy in the bulk or diffuse along the crystalline boundaries.[22] The transport of oxygen in solid oxide fuel cell (SOFC) electrodes with $ABO_3$ type perovskite structure has been studied extensively.[23−25] The above adsorption or diffusion process of oxygen molecules may also exist for the $MIn_{0.5}Nb_{0.5}O_3$ photocatalysts. On the other hand, the NiO-covered Ni layer on the surface of the photocatalyst powder may be oxidized by the photogenerated holes for the $CaIn_{0.5}Nb_{0.5}O_3$ and $SrIn_{0.5}Nb_{0.5}O_3$ photocatalysts during the photocatalytic reactions. Further experiments should be performed to determine which mechanism is dominating the $O_2$ evolution ability for these photocatalysts.

**3.4. Photocatalytic Reactions under Visible Light Irradiation.** The formation rates of $H_2$ evolution from $CH_3OH/H_2O$ solution with cocatalyst Pt (0.2 wt %) under visible light irradiation ($\lambda > 420$ nm) with the $CaIn_{0.5}Nb_{0.5}O_3$, $SrIn_{0.5}Nb_{0.5}O_3$, and $BaIn_{0.5}Nb_{0.5}O_3$ photocatalysts are about 0.28, 0.23, and 0.38 $\mu$mol/h, respectively. The formation rates of $O_2$ evolution from $AgNO_3$ solution without any cocatalyst under visible light irradiation ($\lambda > 420$ nm) with the $CaIn_{0.5}Nb_{0.5}O_3$, $SrIn_{0.5}Nb_{0.5}O_3$, and $BaIn_{0.5}Nb_{0.5}O_3$ photocatalysts are about 0.11, 0.04, and 0.24 $\mu$mol/h, respectively.

The photocatalytic reactions were also performed on the $NiO_x$-loaded $CaIn_{0.5}Nb_{0.5}O_3$, $SrIn_{0.5}Nb_{0.5}O_3$, and $BaIn_{0.5}Nb_{0.5}O_3$ photocatalysts under visible light irradiation ($\lambda > 420$ nm), as shown in Figure 5, where the "dark" experiments were performed on every sample during which the stirring process was kept on and

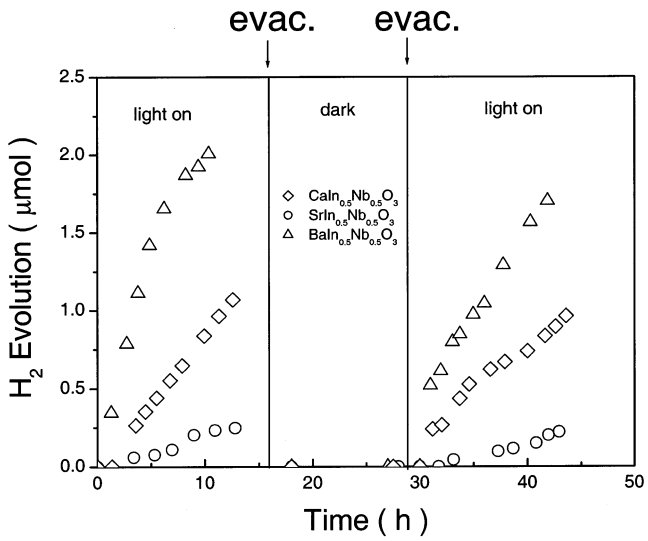


**Figure 5.** Formation rates of $H_2$ evolution from the $NiO_x$-loaded $CaIn_{0.5}Nb_{0.5}O_3$, $SrIn_{0.5}Nb_{0.5}O_3$, and $BaIn_{0.5}Nb_{0.5}O_3$ particles suspended in pure water under visible light irradiation (catalyst: 0.5 g; $NiO_x$, 1.0 wt %; $H_2O$, 270 mL; $\lambda > 420$ nm).

the Xe arc lamp was turned off. In both "light on" runs for the $H_2$ evolution reactions, the $CaIn_{0.5}Nb_{0.5}O_3$, $SrIn_{0.5}Nb_{0.5}O_3$, and $BaIn_{0.5}Nb_{0.5}O_3$ photocatalysts almost had the same $H_2$ formation rates: 0.09, 0.02, and 0.18 $\mu$mol/h, respectively. No $O_2$ evolution was observed. During dark experiments, no gas evolution was obtained, indicating that all of these gas evolutions are from visible light absorption.

The photocatalytic activities of the $CaIn_{0.5}Nb_{0.5}O_3$, $SrIn_{0.5}Nb_{0.5}O_3$, and $BaIn_{0.5}Nb_{0.5}O_3$ photocatalysts in the case of the sacrificial reagents and $NiO_x$ cocatalyst are listed in Table 2. It is obvious from Table 2 that the photocatalytic activities in evolving $H_2$ or $O_2$ from water in the case of the sacrificial reagents and cocatalyst $NiO_x$ under visible light irradiation ($\lambda > 420$ nm) for the $CaIn_{0.5}Nb_{0.5}O_3$, $SrIn_{0.5}Nb_{0.5}O_3$, and $BaIn_{0.5}Nb_{0.5}O_3$ photocatalysts show the following sequence:

$$BaIn_{0.5}Nb_{0.5}O_3 > CaIn_{0.5}Nb_{0.5}O_3 > SrIn_{0.5}Nb_{0.5}O_3 \quad (2)$$

The difference in their photocatalytic activities under visible light irradiation may be related to the band gaps of these photocatalysts corresponding to the visible light absorption, which is dominated by the electronic excitations from the O 2p states to the In 5s states.

As listed in Table 2, the photocatalytic activities of the $CaIn_{0.5}Nb_{0.5}O_3$, $SrIn_{0.5}Nb_{0.5}O_3$, and $BaIn_{0.5}Nb_{0.5}O_3$ photocatalysts under visible light irradiation are very low. To identify whether the $H_2$ evolution reactions under visible light irradiation for these photocatalysts are photocatalytic, the following experiments were also performed. First, we checked the formation rates of $H_2$ evolution from $CH_3OH/H_2O$ solution with 0.2 wt % Pt cocatalyst and without any photocatalyst powder under visible light irradiation ($\lambda > 420$ nm). No $H_2$ evolution could be observed in this blank experiment, indicating that the $H_2$ that evolved in the case of the $CH_3OH/H_2O$ sacrificial reagent are all contributed by the $CaIn_{0.5}Nb_{0.5}O_3$, $SrIn_{0.5}Nb_{0.5}O_3$, and $BaIn_{0.5}Nb_{0.5}O_3$ photocatalysts under visible light irradiation. Second, the wavelength dependence of the $H_2$ formation rate from $CH_3OH/H_2O$ solution with 0.2 wt % Pt cocatalyst for $BaIn_{0.5}Nb_{0.5}O_3$ was investigated with a quartz cell using different cutoff filters, as shown in Figure 6. As a comparison, the wavelength dependence of the $H_2$ formation rate from $CH_3OH/H_2O$ solution with 0.1 wt % Pt cocatalyst for $TiO_2$(P-25) is also

**TABLE 1: Physical Properties and Lattice Parameters of the $CaIn_{0.5}Nb_{0.5}O_3$, $SrIn_{0.5}Nb_{0.5}O_3$, and $BaIn_{0.5}Nb_{0.5}O_3$ Photocatalysts**

| compd | structure | group | tolerance factor | lattice param (nm) | cell volume ($nm^3$) | band gap (eV) |
|---|---|---|---|---|---|---|
| $CaIn_{0.5}Nb_{0.5}O_3$ | orthorhombic | *Pnma* | 0.99 | $a = 0.5532$<br>$b = 0.5715$<br>$c = 0.7918$ | 0.250 | 4.17 |
| $SrIn_{0.5}Nb_{0.5}O_3$ | cubic | *Pm3m* | 0.93 | $a = 0.40569$ | 0.067 | 3.96 |
| $BaIn_{0.5}Nb_{0.5}O_3$ | cubic | *Pm3m* | 0.90 | $a = 0.41454$ | 0.071 | 3.51 |

**TABLE 2: Photocatalytic Activities in Evolving $H_2$ and $O_2$ from Pure Water for the $CaIn_{0.5}Nb_{0.5}O_3$, $SrIn_{0.5}Nb_{0.5}O_3$, and $BaIn_{0.5}Nb_{0.5}O_3$ Photocatalysts under UV and Visible Light Irradiation ($\lambda$ > 420 nm)**

| | | | activity ($\mu$mol/h) | | | |
|---|---|---|---|---|---|---|
| | | | UV | | visible | |
| compd | co-catalyst | condition of water | $H_2$ | $O_2$ | $H_2$ | $O_2$ |
| $CaIn_{0.5}Nb_{0.5}O_3$ | Pt | 50 mL $CH_3OH$ | 304 | | 0.28 | |
| | none | 5mmol $AgNO_3$ | | 6.9 | | 0.11 |
| | $NiO_x$ | pure water | 14.8 | | 0.09 | |
| $SrIn_{0.5}Nb_{0.5}O_3$ | Pt | 50 mL $CH_3OH$ | 57.2 | | 0.23 | |
| | none | 5mmol $AgNO_3$ | | 12.0 | | 0.04 |
| | $NiO_x$ | pure water | 13.8 | | 0.02 | |
| $BaIn_{0.5}Nb_{0.5}O_3$ | Pt | 50 mL $CH_3OH$ | 51.1 | | 0.38 | |
| | none | 5mmol $AgNO_3$ | | 1.2 | | 0.254 |
| | $NiO_x$ | pure water | 27.0 | 12.3 | 0.18 | |

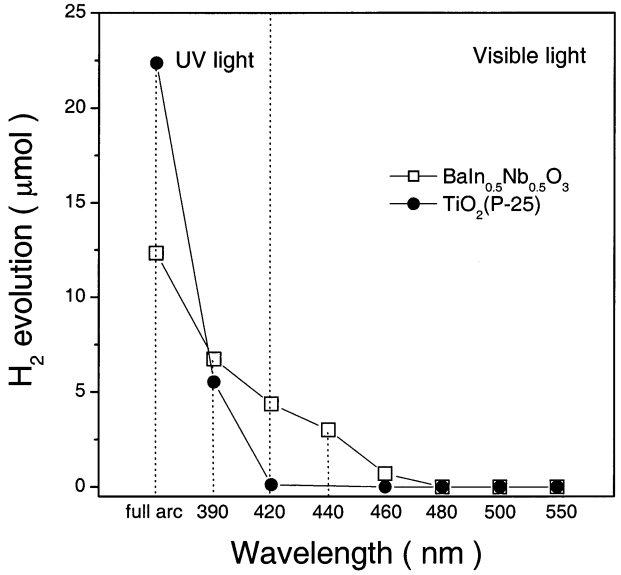


**Figure 6.** Wavelength dependence of the $H_2$ formation rate from $CH_3OH/H_2O$ solution with Pt cocatalyst for the $BaIn_{0.5}Nb_{0.5}O_3$ (0.5 g catalyst, 0.2 wt % Pt, 50 mL of $CH_3OH$, 220 mL of $H_2O$; time, 10 h) and the $TiO_2$(P-25) photocatalyst (0.1 g catalyst, 0.1 wt % Pt, 50 mL of $CH_3OH$, 220 mL of $H_2O$; time, 10 h).

plotted in Figure 6. The number of the incident photons was increased as the wavelength of the cutoff filters was shortened. The photocatalytic activity could not be obtained on $TiO_2$ under visible light irradiation ($\lambda$ > 420 nm), while an obvious photocatalytic activity could be observed on $BaIn_{0.5}Nb_{0.5}O_3$, indicating that the $BaIn_{0.5}Nb_{0.5}O_3$ photocatalyst can respond to visible light irradiation. It is also obvious from Figure 6 that the photocatalytic activity of $BaIn_{0.5}Nb_{0.5}O_3$ disappears when the wavelength of the cutoff filter is larger than 460 nm. This result is consistent with the UV−vis diffuse reflectance spectrum of $BaIn_{0.5}Nb_{0.5}O_3$. So, it is reasonably concluded that the photocatalytic activities of the $CaIn_{0.5}Nb_{0.5}O_3$, $SrIn_{0.5}Nb_{0.5}O_3$, and $BaIn_{0.5}Nb_{0.5}O_3$ photocatalysts observed in our experiments under visible light irradiation are ascribed to visible light absorption.

In summary, new $ABO_3$ type perovskite photocatalysts $CaIn_{0.5}Nb_{0.5}O_3$, $SrIn_{0.5}Nb_{0.5}O_3$, and $BaIn_{0.5}Nb_{0.5}O_3$ with B sites occupied by two metals in a CBM were synthesized. The photophysical properties and the photocatalytic activities under UV and visible light irradiation ($\lambda$ > 420 nm) were investigated. The photoabsorption behaviors of these photocatalysts are related to their band structures, which are thought to be composed of O 2p, In 5s, and Nb 4d states. With the decrease of the ionic radius in the A site, the three photocatalysts showed different photocatalytic activities in evolving $H_2$ and $O_2$ from water under UV and visible light irradiation, respectively. Although the photocatalytic activities of these photocatalysts under visible light irradiation are still low presently, it is a new route to design new photocatalysts responding to visible light irradiation with the CBM method.

**Acknowledgment.** One of the authors (Dr. J. Yin) would like to thank Dr. H. Abe for his help in the experiments, and thank the Japan Society for the Promotion of Science (JSPS) fellowship for financial support.

## References and Notes

(1) Honda, K.; Fujishima, K. *Nature* **1972**, *238*, 37.
(2) Domen, K.; Kudo, A.; Onishi, T. *J. Catal.* **1986**, *102*, 92.
(3) Kudo, A.; Kato, H.; Nakagawa, S. *J. Phys. Chem. B* **2000**, *104*, 571.
(4) Xu, J.; Greenblatt, M. *J. Solid State Chem.* **1996**, *121*, 273.
(5) Sayama, K.; Yase, K.; Arakawa, H.; Asakura, K.; Tanaka, T.; Domen, K.; Onishi, T. *J. Photochem. Photobiol. A* **1998**, *114*, 125.
(6) Kim, H. G.; Hwang, D. W.; Kim, J.; Kim, Y. G.; Lee, J. *J. Chem. Commun.* **1999**, 1077.
(7) Domen, K.; Kondo, J. N.; Hara, M.; Takata, T. *Bull. Chem. Soc. Jpn*. **2000**, *73*, 1307.
(8) Gao, X. S.; Chen, X. Y.; Yin, J.; Wu, J.; Liu, Z. G. *J. Mater. Sci*. **2000**, *35*, 5421.
(9) Goodenough, J. B.; Lango, J. M. *Landolt-Boornstein Tabellen, New Series*; Springer: Berlin, 1970; Vol. III/4a.
(10) Yoo, J.; Lee, Y.; Yoon, K.; Hwang, S.; Suh, S.; Kim, J.; Yoo, C. *Jpn. J. Appl. Phys.* **2001**, *40*, 3256.
(11) Lide, D. R. *Handbook of Chemistry and Physics*, 80th ed.; CRC Press LLC: Boca Raton, FL, 1999.
(12) Kim, H. G.; Hwang, D. W.; Kim, J.; Kim, Y. G.; Lee, J. *J. Chem. Commun.* **1999**, 1077.
(13) Scaife, D. E. *Sol. Energy* **1980**, *25*, 41.
(14) Odaka, H.; Iwata, S.; Taga, N.; Ohnishi, S.; Kaneta, Y.; Shigesato, Y. *Jpn. J. Appl. Phys.* **1997**, *36* (9A), 5551.
(15) Schinzer, C.; Heyd, F.; Mater, S. F. *J. Mater. Chem.* **1999**, *9*, 1569.
(16) Oosawa, Y.; Takahashi, R.; Yonemura, M.; Sekine, T.; Goto, Y. *New J. Chem*. **1989**, *13*, 435.
(17) Lawless, D.; Serpone, N.; Meisel, D. *J. Phys. Chem.* **1991**, *95*, 5166.
(18) Goldstein, S.; Czapski, G.; Rabani, J. *J. Phys. Chem.* **1994**, *98*, 6586.
(19) Yanagisawa, Y.; Ota, Y. *Surf. Sci.* **1991**, *254*, L433.
(20) Lu, G.; Amy, L.; Yates, J. T., Jr. *Chem. Rev*. **1995**, *102*, 3005.
(21) Zou, Z.; Ye, J.; Arakawa, H. *J. Mol. Catal. A: Chem*. **2001**, *168*, 289.
(22) Svensson, A. M.; Sunde, S.; Nisancioglu, K. *J. Electrochem. Soc.* **1998**, *145*, 1390.
(23) van Doorn, R. H. E.; Fuularton, I. C.; de Souza, R. A.; Kilner, J. A.; Bouwmeester, H. J. M.; Burggraaf, A. J. *Solid State Ionics* **1997**, *96*, 1.
(24) Yasuda, I.; Ogasawara, K.; Hishinuma, M.; Kawada, T.; Dokiya, M. *Solid State Ionics* **1996**, *86*, 1197.
(25) Liu, M. *J. Electrochem. Soc*. **1998**, *145*, 142.